Kinetic Characterization of an Organic Radical in the Ascarylose Biosynthetic Pathway†

David A. Johnson,‡ George T. Gassner,§ Vahe Bandarian,|| Frank J. Ruzicka,|| David P. Ballou,§ George H. Reed,|| and Hung-wen Liu*,‡

Department of Chemistry, University of Minnesota, Minneapolis, Minnesota 55455, Department of Biological Chemistry, University of Michigan, Ann Arbor, Michigan 48109-0606, and The Institute for Enzyme Research, Graduate School, and Department of Biochemistry, College of Agricultural and Life Sciences, University of Wisconsin, Madison, Wisconsin 53705

Received June 10, 1996⊗

ABSTRACT: The lipopolysaccharide of *Yersinia pseudotuberculosis V* includes a 3,6-dideoxyhexose, ascarylose, as the nonreducing end of the O-antigen tetrasaccharide. The C-3 deoxygenation of CDP-6-deoxy-L-*threo*-D-*glycero*-4-hexulose is a critical reaction in the biosynthesis of ascarylose. The first half of the reaction is a dehydration catalyzed by CDP-6-deoxy-L-*threo*-D-*glycero*-4-hexulose-3-dehydrase (E_1), which is PMP-dependent and contains a redox-active [2Fe-2S] center. The second half is a reduction that requires an additional enzyme, CDP-6-deoxy-L-*threo*-D-*glycero*-4-hexulose-3-dehydrase reductase (E_3, formerly known as CDP-6-deoxy-$\Delta^{3,4}$-glucoseen reductase), which has a FAD and a [2Fe-2S] center in the active site. Using NADH as the reductant in the coupled E_1-E_3 reaction, we have monitored the kinetics of a radical intermediate using both stopped-flow spectrophotometry and rapid freeze−quench EPR under aerobic and hypoxic conditions. In the EPR studies, a sharp signal at $g = 2.003$ was found to appear at a rate which is kinetically competent, reaching its maximum intensity at ∼150 ms. Stopped-flow UV−vis analysis of the reaction elucidated a minimum of six optically distinguishable states in the mechanism of electron transfer from NADH to substrate. Interestingly, one of the detected intermediates has a time course nearly identical to that of the radical detected by rapid freeze−quench EPR. The difference UV−vis spectrum of this intermediate displays a maximum at 456 nm with a shoulder at 425 nm. Overall, these results are consistent with an electron transfer pathway that includes a radical intermediate with the unpaired spin localized on the substrate−cofactor complex. Evidence in support of this mechanism is presented in this report. These studies add the PMP−glucoseen radical to the growing list of mechanistically important bioorganic radical intermediates that have recently been discovered.

The O-antigen component of lipopolysaccharide (LPS) is a polymorphic oligosaccharide that confers immunological characteristics to many Gram-negative bacteria. Of a variety of sugars present in the O-antigen (Bishop & Jennings, 1982; Kenne & Lindberg, 1983; Raetz, 1990), the 3,6-dideoxyhexoses have been found to bestow the most varied immunogenic properties (Lüderitz et al., 1966; Williams & Wander, 1980), and considerable research has been devoted to elucidate both the genetics and the enzymatic formation of these unusual sugars in recent years (Liu & Thorson, 1994; Liu et al., 1991). So far only five of the eight possible 3,6-dideoxyhexose isomers have been discovered in nature, and the biosynthesis of ascarylose by *Yersinia pseudotuberculosis V* is the best understood (Liu & Thorson, 1994).

Shown in Scheme 1 is an overview of CDP−ascarylose (**1**) biosynthesis with the intriguing C-3 deoxygenation step emphasized. This step consists of a pyridoxamine 5′-phosphate (PMP)-mediated dehydration and an NADH-dependent reduction in which the C-3 hydroxyl group is replaced by a hydrogen (Rubenstein & Strominger, 1974a,b). This deoxygenation event is catalyzed by the sequential actions of two enzymes: CDP-6-deoxy-L-*threo*-D-*glycero*-4-hexulose-3-dehydrase (E_1)[1] and CDP-6-deoxy-L-*threo*-D-*glycero*-4-hexulose-3-dehydrase reductase (E_3, or E_1 reductase, formerly known as CDP-6-deoxy-$\Delta^{3,4}$-glucoseen reductase). It has been shown that E_1 is a unique PMP-dependent enzyme (Rubenstein & Strominger, 1974a; Weigel et al., 1992a,b) that also contains an adrenodoxin/putidaredoxin-like [2Fe-2S] center (Thorson & Liu, 1993a). Our characterization of E_3 revealed that this enzyme includes a FAD and a plant−ferredoxin type [2Fe-2S] center (Miller et al., 1993; Lo et al., 1994). Passage of two electrons from NADH through these iron centers to reduce the dehydration product (species **4** in Scheme 1) must involve radical intermediates since these iron−sulfur centers are one-electron

† Supported by U.S. Public Service Grant GM20877 to D.P.B., NIH Grant GM35906 to H.-w.L., and NIH Grant GM35752 to G.H.R. H.-w.L. is a recipient of a NIH Research Career Development Award (GM00559). D.A.J. is a trainee of a NIGMS Biotechnology Training Grant (GM08347).

* To whom correspondence should be addressed.
‡ University of Minnesota.
§ University of Michigan.
|| University of Wisconsin.

⊗ Abstract published in *Advance ACS Abstracts,* November 15, 1996.

[1] Abbreviations: [2Fe-2S], two iron, two sulfur redox center; AdoMet, 5′-adenosylmethionine; CDP, cytidine 5′-phosphate; DEAE, (diethylamino)ethyl; E_1, CDP-6-deoxy-L-*threo*-D-*glycero*-4-hexulose-3-dehydrase; E_3, CDP-6-deoxy-L-*threo*-D-*glycero*-4-hexulose-3-dehydrase reductase, or E_1 reductase; E_{ep}, CDP-3,6-dideoxy-D-*glycero*-D-*glycero*-4-hexulose-5-epimerase; E_{od}, CDP-D-glucose-4,6-dehydratase; E_{red}, CDP-3,6-dideoxy-L-*glycero*-D-*glycero*-4-hexulose-4-reductase; EPR, electron paramagnetic resonance; FAD or FAD_{ox}, oxidized flavin adenine dinucleotide; FAD_{sq}, semiquinone flavin adenine dinucleotide; FAD_{hq}, reduced flavin adenine dinucleotide hydroquinone; FPLC, fast protein liquid chromatography; PCD, protocatechuate-3,4-dioxygenase; PCA, protocatechuate; PLP, pyridoxal 5′-phosphate; PMP, pyridoxamine 5′-phosphate; RFQ-EPR, rapid freeze−quench electron paramagnetic resonance.

S0006-2960(96)01370-0 CCC: $12.00

Scheme 1: Overview of the Ascarylose Biosynthetic Pathway[a]

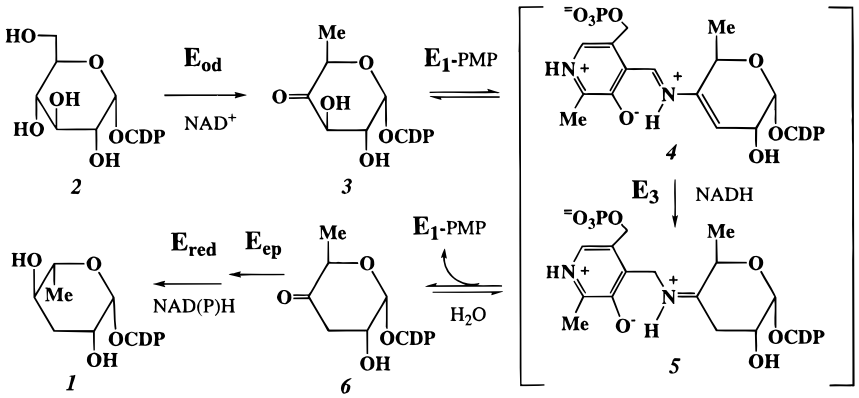

[a] The reaction enclosed in brackets is catalyzed by the E_1-E_3 system.

carriers. Indeed, studies of the reduction of E_3 by NADH have revealed the formation of a flavin semiquinone radical resulting from a single electron transfer from the flavin hydroquinone to the [2Fe-2S] center of E_3 (Gassner et al., 1996).

Previous studies of the reduction of E_1 with dithionite in the presence of substrate (compound **3** in Scheme 1) had afforded preliminary EPR evidence for the formation of a radical intermediate (Thorson & Liu, 1993b). Dithionite was used as a reducing agent instead of E_3 and NADH to avoid any complication in the EPR signals caused by the cogeneration of the flavin semiquinone from E_3. Since this signal did not appear when either substrate or one of the E_1 cofactors was lacking, it is proposed to arise from a PMP−glucoseen-based radical, which is generated during catalytic turnover.

In this paper, we present studies of the reaction of the E_1-E_3 system with the natural substrates NADH and CDP-6-deoxy-L-*threo*-D-*glycero*-4-hexulose (**3**). We used both stopped-flow spectrophotometry and rapid freeze−quench EPR spectroscopy (RFQ-EPR) to study the characteristics and time courses for the formation and decay of intermediates. The results obtained from these complementary experiments also provided further insights into the possible nature of the organic radical.

MATERIALS AND METHODS

Enzyme Purification. E_1 was purified from a previously constructed overproducing *E. coli* JM105/pJT18 strain (Thorson et al., 1994). The purification followed a published procedure (Lei et al., 1995), except for the addition of an FPLC (Pharmacia, Piscataway, NJ) step after the DEAE-Sepharose (Pharmacia) chromatography. The FPLC was equipped with a MonoQ 10/10 anion exchange column (Pharmacia), and the buffers used were A (20 mM Tris-HCl, pH 7.5) and B (1 M NaCl in A, pH 7.5). The elution profile was 0−1 min at 0% B, 1−25 min from 33% B to 50% B, 25−30 min at 70% B, and 30−35 min at 0% B with a flow rate of 3 mL/min. The peaks were monitored at 280 nm and collected manually, concentrated using an Amicon (Danvers, MA) ultrafiltration unit (YM-10 membrane), aliquoted, flash frozen in liquid N_2, and stored at −80 °C. E_3 was purified, with minor modifications, from an overproducing *E. coli* JM105/pOP1 strain as described previously (Ploux et al., 1995). The modifications were as follows: (1) buffer A was 20 mM Tris-HCl (pH 7.5) containing 1 mM β-mercaptoethanol and 0.1 mM EDTA, and buffer B was buffer A containing 0.3 M NaCl; (2) the active fractions after the DEAE-Sepharose step were pooled and concentrated using an Amicon ultrafiltration unit (YM-10 membrane); (3) the MonoQ FPLC purification utilized a linear gradient from 0.16 to 0.36 M NaCl (20 mM Tris-HCl, pH 8.0) in 12 min at a flow rate of 3 mL/min. The molar extinction at 455 nm for E_3 is 22 500 M^{-1} cm^{-1}, and that for E_1 was estimated to be 5450 M^{-1} cm^{-1} (Burns et al., 1996).

Enzyme Assays. Protein concentrations were routinely determined by the Bradford method (Bradford, 1976) using bovine serum albumin (Sigma, St. Louis, MO) as the standard. The Bradford reagent was from Bio-Rad (Richmond, CA). The protein assay was calibrated by comparing the results from quantitative amino acid analysis (Tarr, 1986) performed by the Microchemical Facility at the Institute of Human Genetics of the University of Minnesota to those from the Bradford assay of aliquots of the same sample. The purity of the enzymes was assessed by SDS−PAGE (Laemmli, 1970) and subsequent densitometric analysis using NIH Image 1.60. The previously described assays for measuring the activities of E_1 (Lei et al., 1995) and E_3 (Ploux et al., 1995) were used. The iron content of both enzymes was quantified using the method of Fish (1988).

Substrate Preparation. The E_1 substrate (**3**, CDP-6-deoxy-L-*threo*-D-*glycero*-4-hexulose) was prepared by incubating 34 mg of CDP-D-glucose (**2**, Sigma) and 0.69 mg of CDP-D-glucose 4,6-dehydratase (E_{od}) in 1.1 mL of 50 mM potassium phosphate buffer, pH 7.5, for 4 h at room temperature. The E_{od} was purified from *E. coli*/pJT8 as previously reported (Thorson et al., 1994). At the end of the enzymatic synthesis of **2**, E_{od} was removed by ultrafiltration using a Centricon-10 (Amicon), and the filtrate was collected. Since the conversion was nearly quantitative (Ploux et al., 1995), this substrate solution was used without further purification. The concentration of the substrate was estimated by mixing 2 μL of the filtrate with 798 μL of 0.1 N NaOH for 20 min at room temperature to develop the chromophore, and then measuring the absorbance at 272 (ϵ = 9.1 mM^{-1} cm^{-1}) and 322 nm (ϵ = 5.6 mM^{-1} cm^{-1}). The resulting concentrations deduced from readings at both wavelengths were averaged, and this value was used for subsequent sample preparation (Thorson et al., 1994).

Stopped-Flow Spectrophotometry. Stopped-flow studies were performed using a Hi-Tech Scientific SF-61 stopped-

flow spectrophotometer configured with both photomultiplier tube detection and diode array detection. The flow cell was oriented for a path length of either 1.5 or 10 mm. The samples were prepared in air-tight tonometers and made anaerobic with repeated cycles between vacuum and anaerobic argon. The instrument was made anaerobic by filling and flushing all syringes, tubing, and valves with anaerobic 100 mM potassium phosphate buffer (pH 7.5) containing 1 μM PCD and 100 μM PCA (Bull & Ballou, 1981). Before the experiment, this PCD/PCA solution was replaced with the sample to be used in the stopped-flow study. One syringe was filled with a solution of E_1, E_3, and CDP-6-deoxy-L-*threo*-D-*glycero*-4-hexulose (species **3** in Scheme 1), while the other syringe contained the NADH solution. All solutions were buffered with 20 mM Tris, pH 7.5. The temperature was controlled using a circulating water bath. Data analysis was performed using nonlinear exponential fitting methods previously described by Gassner et al. (1994).

Preparation of Freeze−Quench EPR Samples. The general principles of the freeze−quench EPR method have been developed by Bray (1961) and Ballou and Palmer (1974), and the experimental method used closely follows that of Beinert et al. (1976). A solution containing the two enzymes and substrate of desired concentrations was made anaerobic by repetitive cycling between vacuum and argon at least 10 times over a period of 20 min. The same treatment was also applied to the NADH solution of desired concentration. These solutions were transferred from the anaerobic glassware to separate air-tight sample syringes in an anaerobic chamber (Coy Laboratory Products, Ann Arbor, MI). The syringes were fitted to a Model 1010 Ram controlled by a computer via a Model 7845 controller (Update Instruments, Madison, WI). Depending on the desired aging time, aging tubes (0.509 mm ID) of different lengths were attached between the Wiskind Grid Mixer (Update Instruments) to the spray nozzle. A chilled isopentane-filled funnel attached to an EPR tube was placed under the spray nozzle. The tube and funnel were maintained at 130−145 K in a custom dewar cooled with liquid nitrogen. A stream of N_2 gas, prechilled with liquid nitrogen, maintained anaerobic conditions at the mouth of the funnel. The freeze−quenched reaction products in the form of ice crystals were packed into the EPR tube, which was kept at 130−145 K. After removal of the excess isopentane by aspiration, the packed samples were stored in liquid nitrogen until ready for measurement by EPR spectroscopy. Aerobic experiments were conducted in a similar manner, except that the samples were not deaerated and the ejected reaction mixtures were collected by simply holding the cold isopentane funnel under the spray nozzle.

EPR Spectroscopy. EPR spectra were recorded at X-band on a Varian E-3 spectrometer. The microwave frequency was calibrated with a Hewlett-Packard X532B frequency meter, and the magnetic field was calibrated with a Varian gaussmeter. A liquid N_2 immersion dewar (Suprasil Quartz, Wilmad Glass Co., Buena, NJ) was used to maintain samples at 77 K. All spectra were obtained using microwave power of 4 mW and a modulation amplitude of 5 G. The spectrometer was interfaced with a PC computer for data acquisition and signal averaging. The *g*-values were calculated from frequency and field values and by direct comparison to a Varian strong pitch standard ($g = 2.0028$).

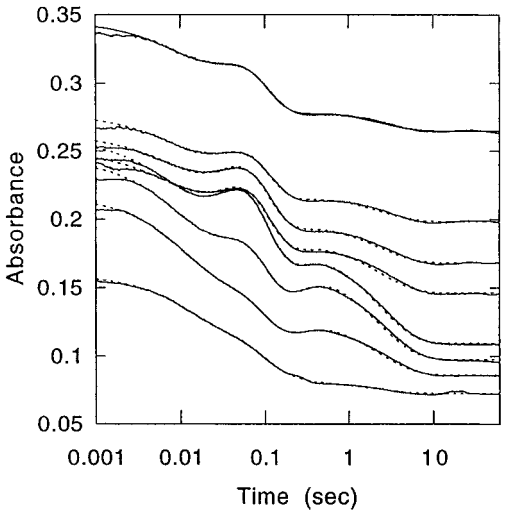

FIGURE 1: Reaction traces recorded at various wavelengths for the reaction of 195 μM E_1, 49 μM E_3, 0.9 mM substrate, and 3.2 mM NADH: (—) actual data, (- - -) calculated exponential fit. By changing only the amplitudes, a set of five rate constants was found that could fit the data at each wavelength: (from top to bottom) 400, 410, 420, 430, 454, 470, 480, and 500 nm.

RESULTS

Enzyme Purification and Characterization. The purity of all enzymes used in the study was at least 95%. The same batches of E_1 (160 nmol min^{-1} mg^{-1}; 1.3 mol Fe/monomer) and E_3 (36 μmol min^{-1} mg^{-1}; 1.6 mol Fe/monomer) were used in both the stopped-flow and the EPR experiments. A separate batch of E_1 (200 nmol min^{-1} mg^{-1}; 1.7 mol Fe/monomer) was used in conjunction with the same E_3 to confirm the line shape and *g*-value of the EPR signals generated under aerobic, steady-state conditions.

Kinetic Study by Stopped-Flow Spectrophotometry. The kinetics of the C-3 deoxygenation catalyzed by E_1 and E_3 at 25 °C were studied under anaerobic conditions. In these studies, an anaerobic solution containing 390 μM E_1, 1.8 mM E_1 substrate, 98 μM E_3, and 20 mM Tris (pH 7.5) was rapidly mixed with an equal volume of an anaerobic solution of 6.3 mM NADH in the same buffer. E_1 and CDP-6-deoxy-L-*threo*-D-*glycero*-4-hexulose (**3**) were present in excess to ensure that all the E_3 was complexed with E_1 and the E_1 substrate was saturating. These relatively high enzyme concentrations were used in order to approximate the conditions used in the EPR experiments discussed below; a 1.5 mm path length flow cell was used in these studies to permit measurements of the sample absorbance. The flavin and iron−sulfur centers in the active sites of E_1 and E_3 have characteristic visible absorption bands that are indicative of their redox states (Miller et al., 1993; Burns et al., 1996); therefore, the progress of the reaction could be followed by monitoring absorbance changes over the full spectral range by diode array detection or at specific wavelengths using photomultiplier tube (PMT) detection. Fitting sequential exponential equations (Gassner et al., 1994) to the PMT data (Figure 1) allowed the determination of the rate constants associated with the changes in absorbance.

Figure 1 clearly shows at least five phases, which implies a minimum of six species being involved. The current data are insufficient to establish the extent of the reversibility of the steps involved in this reaction mechanism. Thus, the rates reported in this paper are the observed rates derived

from fits that assume a linear mechanism composed of irreversible steps. The theoretical time course for the formation and decay of each kinetically distinct intermediate based on the kinetic constants fitted is shown in Figure 2A, and diode array spectra recorded at the maximum accumulation of each intermediate are shown in Figure 2B. Some of the unique characteristics of the intermediate spectra are emphasized in Figure 2C, which is a set of difference spectra obtained by subtracting the 15 s spectrum of the essentially fully reduced E_1-E_3 system from each of the other transient spectra shown in Figure 2B. It should be noted that given the relative rate constants determined for these processes, none of the observed intermediates is a single species; all spectra represent mixtures of species. Scheme 2 presents a logical progression of electron transfers consistent with the spectral data and the redox properties of the cofactors involved. The following is a detailed analysis of each postulated intermediate and its associated rates of formation and decay.

Assignment of Putative Intermediates. The spectrum of the initial E_1-E_3 complex (Figure 2B, dotted line) was recorded before the enzymes were reacted with NADH, and it is composed of the spectra of oxidized E_1 and E_3 (Weigel et al., 1992b; Miller et al., 1993; Lo et al., 1994) complexed together with substrate. In this spectrum, absorbances from both the E_1 and E_3 iron−sulfur centers and the PMP−substrate Schiff base are superimposed on the spectrum of the oxidized FAD of E_3. After mixing with NADH, the absorbance in the 400−500 nm range decreases at 71 s^{-1} in the first kinetically distinct phase. On the basis of studies of the reductive half-reaction of E_3 (Gassner et al., 1996), this loss is consistent with NADH binding, hydride transfer, and intramolecular electron transfer within the E_3 component of the enzyme−substrate complex. As has been shown during the reduction of E_3 by NADH (Gassner et al., 1996), we propose that the release of NAD^+ gates the intramolecular electron transfer and that excess NADH binds to the reduced iron−sulfur and flavin semiquinone-containing intermediate state of the enzyme after the release of NAD^+. These first steps are reflected in Scheme 2 up to the formation of Int-III, which has a maximum accumulation at 21 ms (Figure 2A).

Int-I represents the enzyme−substrate complex bound to NADH, and it is converted to Int-II in a rapid hydride transfer step. Because of the reaction rates, both intermediates are largely missed in the diode array experiment, though the initial ~1 ms diode array spectrum (Figure 2B) is a rough representation of Int-II. Nevertheless, absorbance decreases in the 400−500 nm region of the ~1 ms spectrum are indicative of FAD reduction. During the conversion of Int-II to Int-III, the absorbance lowers further in the 400−600 nm region in Figure 2B due to loss of [2Fe-2S] center absorbance caused by intramolecular electron transfer in E_3.

Subsequent intermolecular electron transfer (38 s^{-1}) leads to Int-IV, which reaches a maximum concentration at 56 ms (Figure 2A). Recent studies of the kinetic properties of E_3 showed that the intramolecular electron transfer between the FAD_{hq} and the [2Fe-2S] center in E_3 is several orders of magnitude faster than the 38 s^{-1} intermolecular electron transfer from E_3 to E_1 (Gassner et al., 1996). Thus, it is likely that the regeneration of the reduced E_3 iron−sulfur center occurs nearly concomitantly with the reduction of the iron−sulfur center of E_1. The consequent reoxidation of

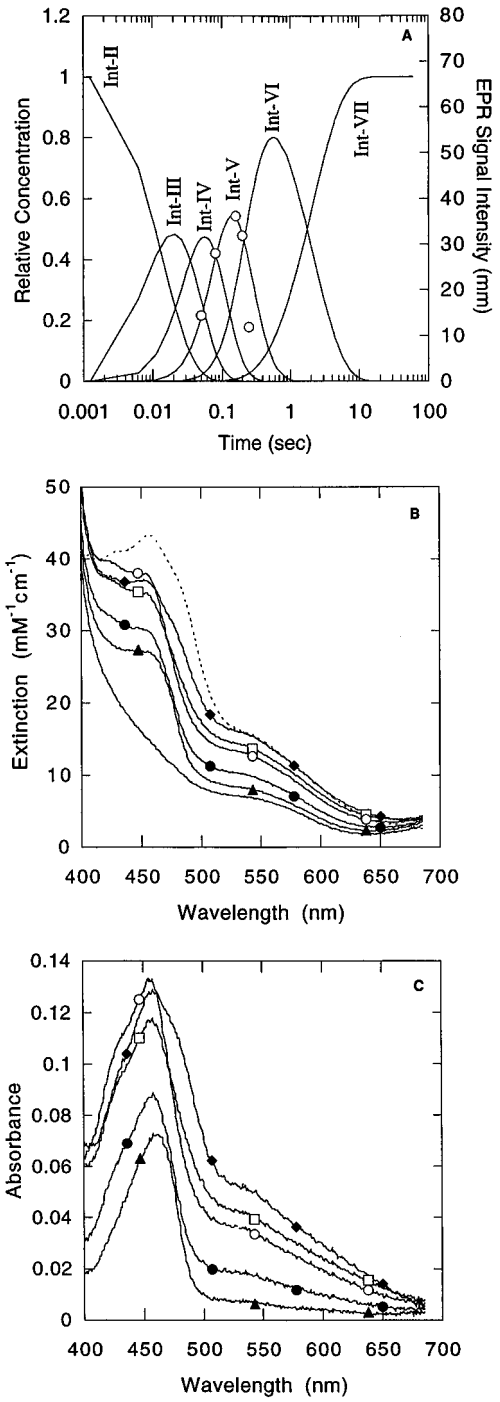

FIGURE 2: Intermediate species in the E_1-E_3-coupled reaction. (A) Concentration profiles calculated from exponential fitting of kinetic data from the reaction of the E_1-E_3 system (Int-II−Int-VII are proposed to correspond to the intermediate structures given in Scheme 2). Radical data from Figure 5 (○) are scaled and overlaid for comparison. (B) Diode array spectra most representative of the reaction intermediates presented in Scheme 2, collected at the times when each of the intermediate concentrations is calculated to be at a maximum: (- - -) Starting oxidized enzyme spectrum, (◆) 1 ms for Int-II, (□) 21 ms for Int-III, (○) 56 ms for Int-IV, (●) 150 ms for Int-V, (▲) 576 ms for Int-VI; (—) 15 s for Int-VII. Enzyme concentrations were used to convert the absorbance to extinction units. (C) Difference spectra of the reaction intermediates depicted in Scheme 2. Each spectrum was obtained by subtracting the 15 s diode array spectrum from each of the other diode array spectra in (B). Symbols are the same as those listed for intermediates in (B).

FAD is observed as an increase in extinction at 454 nm (compare 21 and 56 ms spectra in Figure 2B). Since NADH

Scheme 2: Proposed Electron Transfer Mechanism for the E_1-E_3-Coupled Reaction[a]

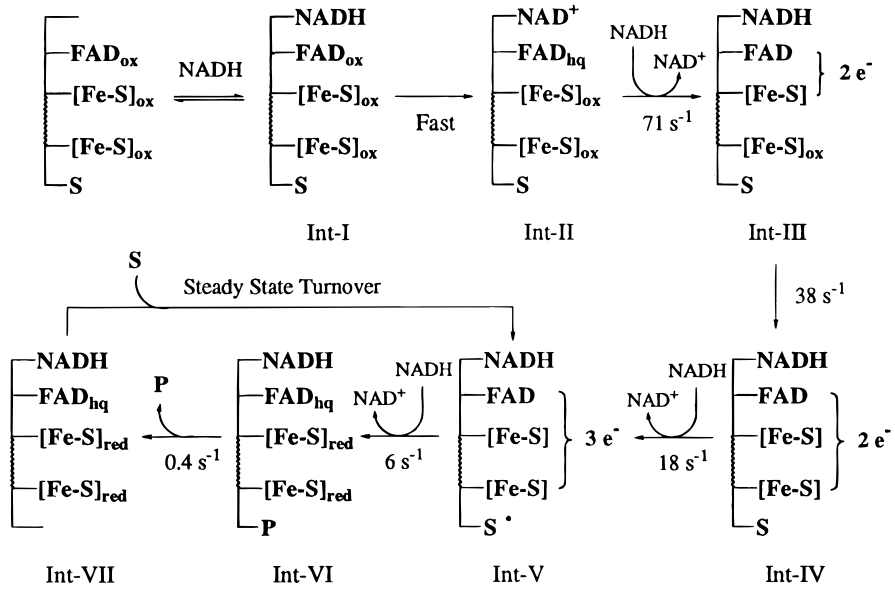

[a] The wavy line represents the interaction between E_1 and E_3 in the enzyme complex. The bracketed cofactors in Int-III, Int-IV, and Int-V indicate unknown dispersal of the designated number of electrons among the cofactors. See text for more details.

was saturating in these studies, spectra of intermediates I, III, and IV (Scheme 2) are expected to include some flavin and reduced pyridine nucleotide charge-transfer absorbance at wavelengths greater than 500 nm (Batie & Kamin, 1986; Massey & Ghisla, 1974). However, the contribution of the charge-transfer absorbance is not clearly discernable because the intense absorbance due to the [2Fe-2S] centers dominates these spectra (Figure 2C). Therefore, our assignment of the pyridine nucleotide charge-transfer state of the E_1-E_3 complex is based on the more discernable charge-transfer absorbance that develops in the reductive half-reaction of E_3 (Gassner et al., 1996).

Loss of both the oxidized FAD in the 400−500 nm range and the oxidized [2Fe-2S] absorbance in the 400−700 nm range ensues at 18 s^{-1} in the transition to Int-V (Scheme 2; Figure 2B). These spectral changes indicate that the flavin and [2Fe-2S] centers are further reduced in Int-V. Analysis of the stopped-flow studies indicates that Int-V accumulates to a maximum concentration at 150 ms, and its formation and decay are nearly the same as those of an organic radical signal detected in EPR studies discussed below. Thus, it is proposed that Int-V represents a four-electron reduced state of the E_1-E_3 system, with one electron residing in the substrate radical and the three remaining electrons dispersed between the FAD and the two [2Fe-2S] centers. The spectrum of Int-V (Figure 2C) has a maximum at 456 nm with a shoulder at 425 nm, with additional absorbance at longer wavelengths due to the flavin semiquinone and reduced [2Fe-2S] centers.

Disappearance of Int-V follows the transfer of a second electron to the E_1 substrate-based radical and results in the formation of Int-VI (6 s^{-1}), which has a maximum concentration at 576 ms (Figure 2A). The overall two-electron reduction from Int-V to Int-VI comprises a series of unresolvable phases, after which the organic radical and the flavin semiquinone are reduced as the E_1-E_3 system consumes an additional equivalent of NADH. In this reaction, there is no transient increase in absorbance in the 400−500 nm range, which would be anticipated for the conversion of FAD_{sq} to FAD_{ox}. We conclude that, in the conversion of Int-V to Int-VI, the rate of reduction of FAD_{ox} by hydride transfer must be significantly greater than the net rate of the single electron transfer reactions that result in the transient oxidation of FAD_{sq}. The spectrum of Int-VI (Figure 2C) has a maximum at 463 nm with no significant absorbance at longer wavelengths.

During the conversion to Int-VII, this absorbance is lost at 0.4 s^{-1}. The spectrum of Int-VII (Figure 2B) consists of reduced FAD and [2Fe-2S] centers, with no other observable chromophores. The absorbance from these reduced cofactors is subtracted from the spectra of Int-V and Int-VI (Figure 2C), so the remaining absorbance from 400−500 nm must derive from another chromophore. These chromophores may be various redox and protonation states of the PMP−substrate Schiff base, and this hypothesis is further addressed in the Discussion. After the first turnover, the enzyme system may cycle between intermediates V, VI, and VII in steady-state turnover as excess substrate is converted to product (Scheme 2). Since product release is slow compared with the electron transfer steps that lead to cofactor reduction, the enzyme system remains substantially reduced during turnover. Finally, as the last of the E_1 substrate is consumed, the concentration of the Schiff base−enzyme complex is depleted and the fully reduced enzyme system accumulates as Int-VII (Scheme 2; Figure 2B).

It should be pointed out that the determination of the exact distribution of electrons between all the cofactors in the E_1-E_3 complex will require a more thorough kinetic and spectroscopic analysis. Because the precise redox state of the cofactors cannot be deduced from the present data, in Scheme 2 we indicate with certainty the direction of the electron flow, but we define somewhat ambiguously the distribution of electrons between the FAD and [2Fe-2S] centers (see the bracketed cofactors in intermediates III, IV, and V).

In a separate study employing both EPR and stopped-flow techniques, the approach to and exit from steady-state turnover were monitored during the reaction of E_3 with a

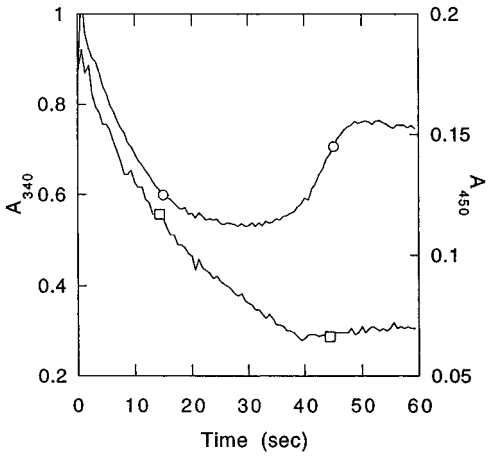

FIGURE 3: Steady-state turnover of the E_1-E_3 system. Reaction of 242 μM E_1, 7 μM E_3, 3.75 mM E_1 substrate, and 750 μM NADH. Changes in enzyme oxidation state monitored at 450 nm (○) and NADH consumption monitored at 340 nm (□) in the Hi-Tech spectrophotometer configured with diode array detection. Single-wavelength traces were extracted from 96 spectra (each spectrum recorded in 1.25 ms) over 60 s.

large excess of E_1 under aerobic conditions in which NADH was limiting with respect to the E_1 substrate (Figure 3). The stopped-flow studies provide further support for the notion that reaction steps associated with product release are limiting in the overall rate of catalysis by showing that E_1 and E_3 remain nearly fully reduced during steady-state turnover. In the first part of the reaction (first 20 s of Figure 3), the absorbance at 450 nm decreases as the population of E_1 becomes increasingly reduced in the approach to steady state. During the steady-state phase of the reaction (between 20 and 40 s), the fully reduced form of the enzymes predominates due to slow product release. At 40 s into the reaction, nearly all the NADH has been consumed (see 340 nm absorbance in Figure 3), and the enzyme system reoxidizes as it continues to react with excess E_1 substrate (note increase in 450 nm absorbance). The EPR data from a reaction conducted under similar aerobic, steady-state conditions are discussed below.

Detection of a Paramagnetic Intermediate by EPR. An EPR signal consistent with that of an organic radical was observed in an earlier EPR study of E_1 in which dithionite was used as the reducing agent (Thorson & Liu, 1993b). We decided to determine in this study whether the same organic radical would appear with E_3 transferring the reducing equivalents from NADH, as in the natural reaction. EPR spectra were recorded after a sample was prepared by vortexing an aerobic reaction mixture of 470 μM E_1, 7.5 μM E_3, 1.1 mM NADH, and 10.3 mM substrate (**3**), quickly transferring the mixture to an EPR tube, and then freezing in liquid N_2 (about 20−30 s total). A control sample lacking substrate was run in parallel. First-derivative and absorption EPR spectra of these samples are shown in Figure 4. It should be noted that while the EPR signal of the reduced iron center of E_3 is prominent at 10−40 K (Miller et al., 1993), it is barely detectable at 77 K under high gain (Figure 4D). Furthermore, since only a catalytic amount of E_3 was used in these experiments, the contribution of its reduced iron center to the EPR signal, if any, should be minimal. Thus, the [2Fe-2S] component of the EPR signal observed in the reaction of the E_1-E_3 system with NADH and E_1 substrate at 77 K derives predominantly from the reduced iron center of E_1.

Shown in Figure 4A is an EPR spectrum that can be attributed to the reduced [2Fe-2S] center ($[2Fe\text{-}2S]_{red}$) in E_1. This spectrum exhibits slightly rhombic symmetry ($g_1 = 2.012$; $g_2 = 1.950$; $g_3 = 1.932$). Interestingly, the spectrum of the sample that contains substrate (Figure 4B) shows an additional signal that overlaps the low-field region of the

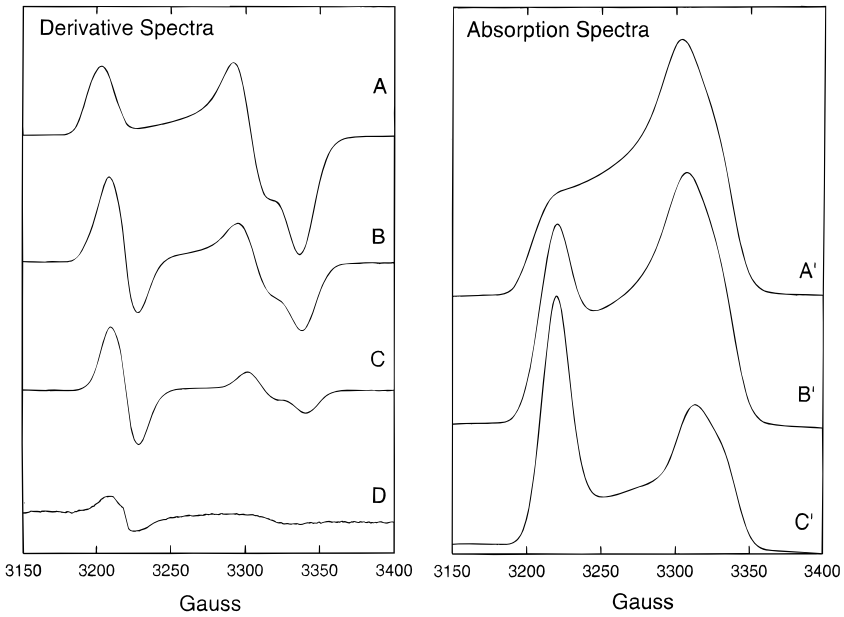

FIGURE 4: EPR spectra in the presence and absence of substrate. These spectra were recorded as the first derivatives on samples prepared from an aerobic reaction of 470 μM E_1, 7.5 μM E_3, 1.1 mM NADH, and (A) no substrate or (B) 10.3 mM substrate. Trace C shows a subtraction of 40% of A from B (raw data). Data were not normalized for differences in gain setting, and 40% represents the maximum amount of iron−sulfur center that could be subtracted without introducing negative lobes into the difference spectrum. Trace D is the EPR spectrum of a control sample prepared by reacting 7.5 μM E_3 with 1.1 mM NADH. Spectra were recorded at a microwave frequency of 9.05 GHz (traces A−C) or 9.045 GHz (trace D). Relative gains were 1, 4, and 5 for traces A, B, and D, respectively, and the temperature was 77 K. The first-derivative spectra were integrated to obtain the absorption mode spectra. Traces A′, B′, and C′ correspond to the derivative spectra A, B, and C, respectively.

spectrum of $[2Fe\text{-}2S]_{red}$. EPR analysis of an aerobic reaction mixture of 7.5 μM E_3 with 1.1 mM NADH also exhibits a weak signal at $g \approx 2.003$ (Figure 4D), which is attributed primarily to the flavin semiquinone generated by the NADH oxidase activity of E_3 in the presence of oxygen (Lo et al., 1994). The semiquinone signal appears to be distorted due to the coexistence of some $[2Fe\text{-}2S]_{red}$ signal. Because the intensity of the semiquinone EPR signal is considerably less than that of the substrate-based organic radical (compare Figure 4D and 4B), the intense radical feature observed in the spectrum of the sample containing substrate is not due to a semiquinone radical in E_3. While one cannot rule out small contributions of the flavin semiquinone radical to the spectra of the samples with and without the substrate, the difference spectrum (Figure 4C) should minimize the contribution of the semiquinone radical and yield a signal due to the substrate-dependent radical, which is centered at $g = 2.003$ and appears to have little g anisotropy. These spectral features are consistent with those of an organic radical as opposed to a [2Fe-2S] species. The detection of this organic radical signal in the EPR spectra strongly supports the proposal that a one-electron reduced form of the substrate−PMP adduct occurs in the reduction of the glucoseen intermediate by E_3 during the deoxygenation catalyzed by E_1, E_3, and NADH.

In addition to the substrate-dependent signal centered at 3220 G in Figure 4C, contributions from the $[2Fe\text{-}2S]_{red}$ center in E_1 remain in the difference spectrum as evidenced by the presence of signals at 3313 G. Furthermore, the presence of residual [2Fe-2S] component in the difference spectrum prevents a meaningful determination of the number of spins per enzyme molecule. The residual spectral contribution from the $[2Fe\text{-}2S]_{red}$ center of E_1 in Figure 4C could result from a substrate-induced change in the spectrum of $[2Fe\text{-}2S]_{red}$ so that a direct subtraction cannot give the pure substrate radical signal. This point is addressed more fully in the Discussion.

Time Course of the EPR Radical Signal. Rapid freeze−quench EPR experiments were carried out to determine the kinetics of the appearance and the decay of the paramagnetic intermediate in the complete E_1−E_3 reaction mixture. To facilitate comparison of the kinetic properties of the paramagnetic intermediate with those of intermediates detected optically, the freeze−quench EPR measurements were conducted anaerobically under conditions nearly identical to those used in the stopped-flow experiments.

Even though the substrate-dependent signal overlaps the low-field region of the $[2Fe\text{-}2S]_{red}$ spectrum, the relative spectral contributions of the two species can be distinguished because of differences in their line shapes. For example, the part of the signal observed at ~3306 G in the first-derivative display is due exclusively to the $[2Fe\text{-}2S]_{red}$ within E_1, while the component of the signal that appears below the base line in the low-field region of the spectrum is solely due to an organic radical. The kinetic profiles of the respective amplitudes of the signals are shown in Figure 5, and the profile for the substrate-dependent component is also overlaid on the optical profiles calculated in Figure 2A. Spectra taken at <50 and >250 ms after mixing did not reveal any different paramagnetic species. The substrate-dependent signal was detectable in samples quenched as early as 25 ms after mixing. The signal of the substrate-dependent species reached maximum amplitude at ~150 ms.

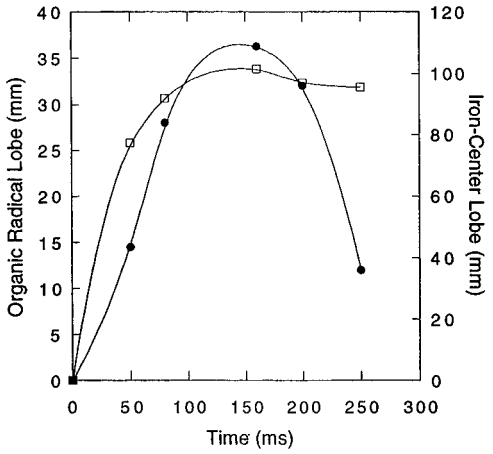

FIGURE 5: EPR time course of the organic radical and E_1 [2Fe-2S] center. The graph depicts the kinetic profile of the organic radical (●) and the E_1 $[2Fe\text{-}2S]_{red}$ (□). Spectra were obtained from an anaerobic reaction mixture of 195 μM E_1, 49 μM E_3, 0.90 mM substrate, and 3.2 mM NADH at room temperature. Reactions were quenched at 50, 80, 160, 200, and 250 ms as described in Materials and Methods and analyzed by EPR as in Figure 4. Amplitudes of organic radical and E_1 $[2Fe\text{-}2S]_{red}$ signals were determined as described in the text and were normalized for the spectrometer gain setting before preparing the plot. Data are fit to smooth curves with no model intended.

DISCUSSION

Electron Transfer through the E_1−E_3-Coupled System. We are unable to completely deduce a single, unique electron transfer pathway from the available spectroscopic data. However, our detailed knowledge of the separate E_1 and E_3 components necessarily limits the number of possible mechanisms involved with the transfer of electrons in the enzyme-coupled reaction. The overall flow of electrons had been determined to be from NADH to E_3 to E_1 (Thorson & Liu, 1993a). Our early studies also clearly characterized the steps of NADH binding, hydride transfer, and intramolecular electron transfer between the FAD and [2Fe-2S] center of E_3 in its reductive half-reaction with NADH (Gassner et al., 1996). Other experiments had established that one-electron reduction of the [2Fe-2S] center of E_1 occurs prior to generation of an organic radical in the presence of substrate (Thorson & Liu, 1993b). Scheme 2 presents a reasonable electron transfer pathway that is both consistent with all the previous work and supported by the current optical and EPR results. However, the extent and reversibility of these electron transfer reactions cannot be deduced accurately from the available data; therefore, the precise distribution of electrons between the FAD and [2Fe-2S] centers is uncertain. In addition, the absorbance characteristics of the various protonation and redox states of E_1-bound PMP remain to be determined, so complete deconvolution of the complex spectra of the intermediates involved in the E_1−E_3 reaction is currently not possible.

Although the spectral contributions of the E_1−substrate radical (Int-V) and the E_1−product complex (Int-VI) are not known, the optical data (Figure 2) are consistent with nearly complete reduction of the FAD of E_3 and the [2Fe-2S] centers of both E_1 and E_3 in these intermediates. Since the stopped-flow experiments were performed under conditions of substrate saturation, all these intermediates are expected to have the sugar substrate or product bound as a Schiff base with PMP in the active site of E_1. Other investigators have

thoroughly characterized various forms of coenzyme B_6 Schiff bases (Schnackerz et al., 1979, 1995; Miles, 1986), and they discovered that the quinonoid forms have a strong absorption in the 450−520 nm range. The fact that intermediates I−VI have a strong absorption from 420 to 470 nm (Figure 2C) allows for the possibility of an enzyme-bound Schiff base for these intermediates. The implication of these wavelength maximums on the detailed radical mechanism will be discussed below.

Formation of a Transient Radical Intermediate. Rapid freeze−quench EPR was utilized to determine whether in the E_1−E_3-catalyzed reaction any paramagnetic species are present with kinetic profiles that can be correlated with those detected optically by stopped-flow spectrophotometry. EPR measurements of rapid freeze−quench samples prepared with similar concentrations as used in the optical experiments demonstrate the development of a short-lived radical species with a maximum free radical signal occurring at ∼150 ms (Figure 5). The kinetic course for the radical did not match that of the E_1 $[2Fe\text{-}2S]_{red}$ center (Figure 5), indicating that the profile obtained for the radical is not an artifact introduced by the overlapping low-field component of the E_1 $[2Fe\text{-}2S]_{red}$ center (Figure 4A). Power saturation behavior confirmed the presence of two independent signals (data not shown). The kinetic profile of the organic radical EPR signal matches that of Int-V determined independently by stopped-flow measurements (Figure 2A). Since Int-V contains both the E_3 semiquinone and the substrate-dependent radical, both species are expected to contribute to this signal, though the ratio of the two species cannot be accurately determined because of the similar *g*-values and the unknown extinction coefficient of the substrate-dependent radical. Scheme 2 shows that Int-V decays at 6 s^{-1}, while Int-VI decays much more slowly (0.4 s^{-1}). Thus, we expect to see a transient accumulation of Int-V followed by a buildup of Int-VI. Figure 5 is entirely consistent with this logic.

The E_1 $[2Fe-2S]_{red}$ contribution to the EPR spectrum could be partially substracted to reveal an isotropic organic radical signal with a *g*-value of 2.003. This value was rigorously verified with two different batches of E_1, so it replaces the previously reported value of 2.007 (Thorson & Liu, 1993b). One possible reason for being unable to cleanly subtract the iron−sulfur component (Figure 4C) may be a change in the environment of the metal center upon binding with substrate. Perhaps the iron−sulfur center is close enough to the substrate-based organic radical to cause some spin−spin interactions that subtly change the EPR properties of the metal center. The validation of this hypothesis must await the three-dimensional structure of the E_1−substrate complex and more detailed EPR analysis. Nonetheless, a relevant precedent for the interaction of an iron−sulfur center with an organic radical is the trimethylamine dehydrogenase case, in which the flavin semiquinone was found to interact with the neighboring [4Fe-4S] center (Stevenson et al., 1986).

The organic radical will form under either aerobic or hypoxic conditions, and the EPR of either a single-turnover or a steady-state sample revealed similar radical signals. However, when the freeze−quench experiments of the E_1−E_3-coupled reaction were carried out aerobically, the maximum spin concentration for the organic radical occurred at ∼80 ms instead of 150 ms. While the kinetic difference is not understood, it may be due to the presence of the competing NADH oxidase reaction. The ability of E_3 to react with oxygen and generate FAD semiquinone may accelerate the electron transfer between the cofactors. Alternatively, oxygen may react with the radical and provide two routes for its decay, one to Int-VI and the other to an oxidized species. Two pathways for the decay of Int-V would have the combined effect of speeding up the disappearance of Int-IV and accelerating the observed appearance of Int-V. Further studies are needed to clarify this phenomenon.

Correlation of Freeze−Quench and Stopped-Flow Data. Direct comparison of the rapid freeze−quench EPR time course data with the sequential exponential fits of the stopped-flow data supports the proposed intermediates (Scheme 2). In the early part of the reaction at 25 ms, the stopped-flow data show that the reaction is composed of a mixture of Int-II, Int-III, and Int-IV, with Int-III being the dominant species (Figure 2A). Therefore, the E_1 [2Fe-2S] is predicted to be still mostly oxidized, which is the case as judged by the relatively small iron center signal in the EPR spectrum (data not shown). Likewise, the stopped-flow data predict that at 50 ms the organic radical starts to accumulate, coinciding with the formation of some Int-V (Figure 2A). The accumulation of organic radical and reduced E_1 [2Fe-2S] signal in the EPR spectrum at 50 ms (Figure 5) is indeed consistent with the conversion of Int-IV to Int-V. Further reduction brings both the organic radical and iron−sulfur EPR signals to their maximum intensity at ∼150 ms, which is also the maximum accumulation of Int-V calculated from analysis of the UV−vis data (Figure 2A). The nearly constant $[2Fe\text{-}2S]_{red}$ EPR signal after 150 ms, when the organic radical signal is decaying, provides evidence for the existence of fully reduced Int-VI and Int-VII. Judging from the results of sequential exponential fitting (Figure 2A), hydrolysis of the PMP−product Schiff base in Int-VI is underway by 1 s. Thus, the fact that the iron centers are still reduced at the longest measured EPR time point of 3.75 s (not shown) indirectly affirms the nature of both Int-VI and Int-VII. Overall, the EPR and stopped-flow data support the mechanism in Scheme 2 for the formation of an organic radical intermediate in this reaction pathway. We note that the calculations used to generate Figure 2A do not completely reflect the experimental conditions. Since accounting for the steady-state cycling through Int-V, Int-VI, and Int-VII would make the modeling unnecessarily complex, the calculations are only for a single turnover. In steady state one would expect all the rates to be similar to those in Scheme 2, though the concentrations would reach fairly constant levels.

Nature of the Radical Species. The kinetically relevant organic radical species observed by rapid freeze−quench EPR during E_1−E_3 catalysis might be either a protein-based radical or a PMP−glucoseen radical as previously surmised (Thorson & Liu, 1993b). If an amino acid residue is directly involved in the electron transfer pathway, it is reasonable to presume that reduction of this residue would precede reduction of the PMP−glucoseen adduct (**4** in Scheme 3), which is the ultimate acceptor in the overall electron relay. Thus, reduction of E_1 either with dithionite or with E_3 plus NADH is expected to activate this putative protein radical and to generate an EPR signal even in the absence of substrate. Such is the case with known protein-based radicals, in which formation of the catalytically essential protein radical can be activated by an external oxidant, autoxidation, or a secondary protein. Examples include the

Scheme 3: Details of the Proposed Radical Generation Mechanism of the E_1-E_3-Coupled Reaction

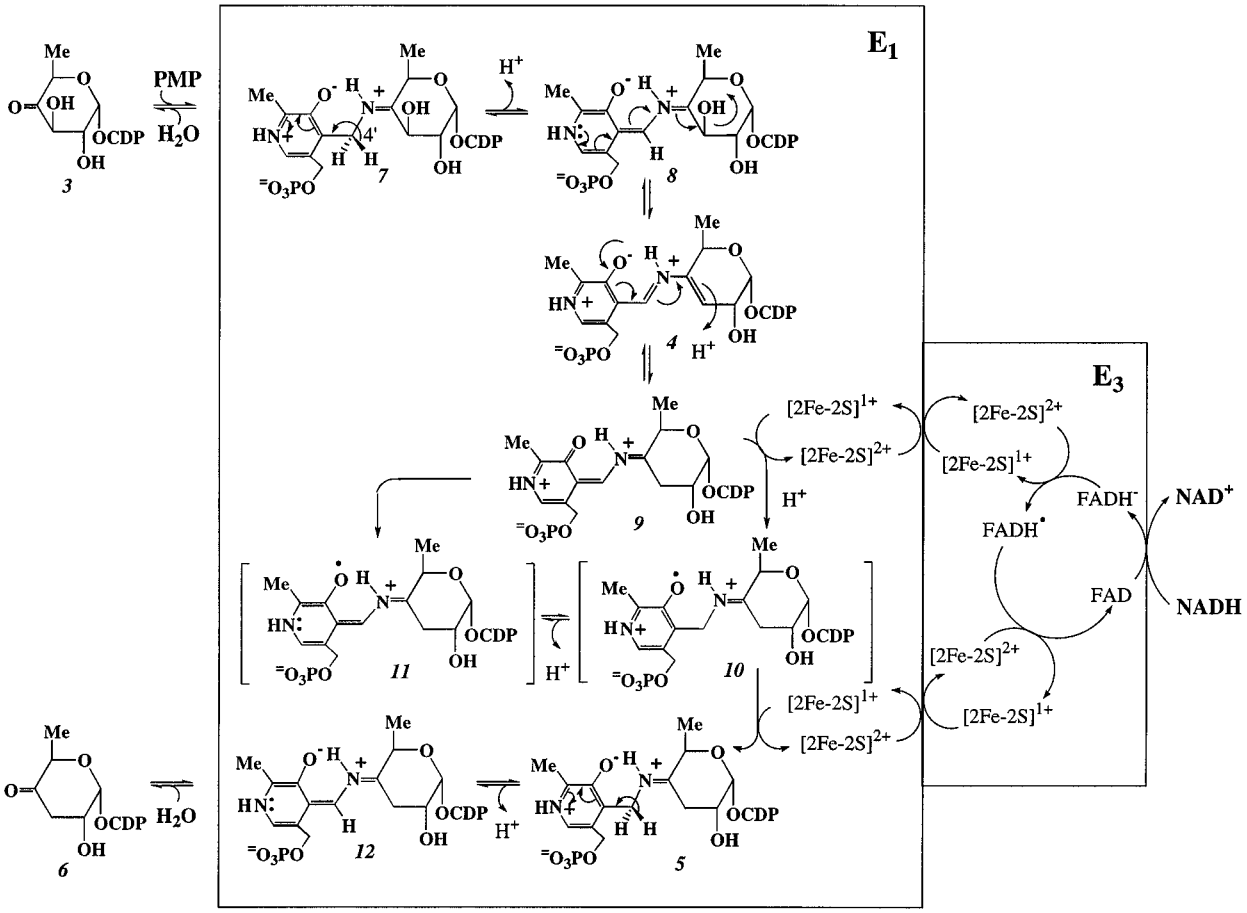

activation of aerobic ribonucleotide reductase with Fe^{2+} and O_2 (Ravi et al., 1994; Bollinger et al., 1994a,b), of anaerobic ribonucleotide reductase by an iron-containing activase (Sun et al., 1995), of pyruvate formate-lyase by an Ado-Met-dependent activase (Wagner et al., 1992; Frey et al., 1994), of amine oxidase by copper-mediated autoxidation (Matsuzaki et al., 1995), of prostaglandin H synthase by hydrogen peroxide (Karthein et al., 1988), and of galactose oxidase by potassium ferricyanide (Whittaker & Whittaker, 1990). Hence, assignment of the observed paramagnetic species at $g = 2.003$ in Figure 4C as a substrate-derived organic radical remains to be the most likely scenario. Two other examples of a cofactor−substrate radical being formed during catalytic turnover include copper amine oxidase (Pedersen et al., 1992; Medda et al., 1995) and lysine 2,3-aminomutase (Ballinger et al., 1992, 1995; Wu et al., 1995).

Proposed Radical Mechanism. The arguments summarized above are consistent with the proposed radical mechanism shown in Scheme 3. Previously, reduction of E_1 with dithionite in the presence of substrate generated an isotropic EPR signal, which led to the hypothesis that reduction of the PMP−glucoseen (**4**) may generate a transient C-3 phenoxy radical on the PMP−substrate complex (Thorson & Liu, 1993b). Though a similar signal was produced in the EPR experiments discussed in this report, the current study was not designed to pinpoint the atom(s) with which the unpaired spin is associated. Nevertheless, the radical intermediate (**10** and/or **11**) depicted in Scheme 3 remains the most reasonable alternative based on the evidence we have presented. Additionally, the PMP−substrate Schiff base **4** can tautomerize into a quinone methide species **9**, and these types of compounds are well-known to be good one-electron acceptors (Wagner & Gompper, 1974; Karabelas & Moore, 1990).

However, the purported unconjugated structure **10**, a PMP−ketimine Schiff base that is expected to absorb in the range 330−335 nm (Torchinsky, 1986), is incompatible with the spectrum of Int-V, which has an absorption maximum at 456 nm (Figure 2C). Interestingly, the spectrum of Int-V resembles that of the substrate−topaquinone radical found in copper amine oxidase (Pedersen et al., 1992), with additional absorbance at longer wavelengths due to the flavin semiquinone and reduced [2Fe-2S] centers. Int-VI also exhibits a long wavelength absorption maximum that appears at 463 nm, and it may arise from a Schiff base between PMP and the deoxy sugar product (**12**). The fact that the λ_{max} of these intermediates undergoes a large shift from the range 330−335 nm typical for PMP−ketimine Schiff bases to 450−460 nm strongly implies a highly conjugated skeleton for these sugar Schiff bases.

The spectral properties of coenzyme B_6 and its reactions with amines and amino acids are well documented (Schnackerz et al., 1979, 1995; Miles, 1986). Comparison with these well-characterized systems implied that a sugar−PMP quinonoid structure is a good candidate for these intermediates. For example, quinonoids generated in PLP-dependent β-elimination reactions commonly absorb in the 450−520 nm range with extinction coefficients as high as 40 mM^{-1} cm^{-1} (Kallen et al., 1985). The strong absorption observed for Int-V and Int-VI in Figure 2C clearly falls into this range. Furthermore, the shoulder at about 425 nm in Int-V is characteristic of *p*-quinonoid structures, which

typically have shoulders around 27 nm from the major peak on the short wavelength side (Kallen et al., 1985). As depicted in Scheme 3, one-electron reduction of species **9** could give species **10** and/or species **11** as the nascent products, which may be interconvertible via proton abstraction from C-4′. Since Int-V exhibits a strong absorbance at 456 nm, the active site of E_1 apparently can stabilize some fraction of the quinonoid form (species **11** in Scheme 3) of the radical. A similar implication may be extended to Int-VI in which species **12**, instead of species **5**, could be a major contributor to the absorption at 463 nm. Because a strong absorption band in the 420−470 nm region is observed for all intermediates in Figure 2C, the PMP−sugar Schiff base intermediates during E_1−E_3 catalysis appear to exist at least partially in the quinonoid form.

Concluding Remarks. Although coenzyme B_6 can participate in amazingly diverse chemistry, its catalytic functions rely primarily on the ability of this cofactor to act as an electron sink, temporarily storing the electrons that are later used for the cleavage and/or formation of covalent bonds. This ability to stabilize anions is utilized by the PMP in the E_1−E_3 system to promote a classical dehydration of CDP-6-deoxy-L-*threo*-D-*glycero*-4-hexulose (**3**). However, E_1-bound PMP also mediates unprecedented one-electron redox chemistry. The combined dehydration and one-electron redox capability place E_1 in its own class, with the C-3 deoxygenation a unique example of a C−O bond cleavage event. Though our studies of this bond cleavage event have added novel radical chemistry to the known functionality of PMP, coenzyme B_6 has long been known to mediate two-electron redox reactions. Specifically, the transamination reaction catalyzed by other PLP/PMP-dependent enzymes is in fact a two-electron redox process, even if coenzyme B_6 is frequently not perceived as a redox cofactor. Thus, these studies not only expand our knowledge of the catalytic diversity of coenzyme B_6 but also emphasize the less recognized redox nature of this common cofactor. It can be noted that the overall reaction catalyzed by the E_1−E_3 system is essentially the same as that catalyzed by ribonucleotide reductase, another enzyme that uses radical chemistry (Stubbe, 1989; Marsh, 1995), although the E_1−E_3 system uses a totally different set of cofactors for this purpose. Interestingly, a coenzyme B_6-dependent dideoxygenation followed by transamination was recently found in the biosynthesis of blasticidin S (Gould & Guo, 1992). It is possible that a similar mechanism is operative in that case. The traditional role of coenzyme B_6 has also been varied by lysine-2,3-aminomutase, which utilizes PLP to catalyze the radical rearrangement of lysine (Ballinger et al., 1992, 1995; Wu et al., 1995). Future research may prove that coenzyme B_6 plays an even more versatile role than was previously surmised.

ACKNOWLEDGMENT

We would like to thank Kirsi Vatanen, currently at Pharmacia, Sweden, for providing the E_{od} enzyme used in the study.

REFERENCES

Ballinger, M. D., Frey, P. A., & Reed, G. H. (1992) *Biochemistry 31*, 10782−10789.
Ballinger, M. D., Frey, P. A., Reed, G. H., & LoBrutto, R. (1995) *Biochemistry 34*, 10086−10093.
Ballou, D. P., & Palmer, G. (1974) *Anal. Chem. 46*, 1248−1253.
Batie, C. J., & Kamin, H. (1986) *J. Biol. Chem. 261*, 11214−11223.
Beinert, H., Hansen, R. E., & Hartzell, C. R. (1976) *Biochim. Biophys. Acta 423*, 339−355.
Bishop, C. T., & Jennings, H. J. (1982) in *The Polysaccharides, Vol. 1* (Aspinall, G. O., Ed.) pp 291−330, Academic Press, New York.
Bollinger, J. M., Jr., Tong, W. H., Ravi, N., Huynh, B. H., Edmondson, D. E., & Stubbe, J. (1994a) *J. Am. Chem. Soc. 116*, 8015−8023.
Bollinger, J. M., Jr., Tong, W. H., Ravi, N., Huynh, B. H., Edmondson, D. E., & Stubbe, J. (1994b) *J. Am. Chem. Soc. 116*, 8024−8032.
Bradford, M. M. (1976) *Anal. Biochem. 72*, 248−254.
Bray, R. C. (1961) *Biochem. J. 81*, 189−193.
Bull, C., & Ballou, D. P. (1981) *J. Biol. Chem. 256*, 12673−12680.
Burns, K. D., Pieper, P. A., Liu, H.-w., & Stankovich, M. T. (1996) *Biochemistry 35*, 7879−7889.
Fish, W. W. (1988) *Methods Enzymol. 158*, 357−364.
Frey, M., Rothe, M., Wagner, A. F. V., & Knappe, J. (1994) *J. Biol. Chem. 269*, 12432−12437.
Gassner, G. T., Wang, L., Batie, C., & Ballou, D. P. (1994) *Biochemistry 33*, 12184−12193.
Gassner, G. T., Johnson, D. A., Liu, H.-w., & Ballou, D. P. (1996) *Biochemistry 35*, 7752−7761.
Gould, S. J., & Guo, J. (1992) *J. Am. Chem. Soc. 114*, 10176−10181.
Kallen, R. G., Korpela, T., Martell, A. E., Matsushima, Y., Metzler, C. M., & Metzler, D. E. (1985) in *Transaminases* (Christen, P., & Metzler, D. E., Eds.) pp 37−108, John Wiley & Sons, New York.
Karabelas, K., & Moore, H. W. (1990) *J. Am. Chem. Soc. 112*, 5372−5373.
Karthein, R., Dietz, R., Nastainczyk, W., & Ruf, H. H. (1988) *Eur. J. Biochem. 171*, 313−320.
Kenne, L., & Lindberg, B. (1983) in *Bacterial Polysaccharides, Vol. 2* (Aspinall, G. O., Ed.) pp 287−363, Academic Press, New York.
Laemmli, U. K. (1970) *Nature (London) 227*, 680−685.
Lei, Y., Ploux, O., & Liu, H.-w. (1995) *Biochemistry 34*, 4643−4654.
Liu, D., Verma, N. K., Romana, L. K., & Reeves, P. R. (1991) *J. Bacteriol. 173*, 4814−4819.
Liu, H.-w., & Thorson, J. S. (1994) *Annu. Rev. Microbiol. 48*, 223−256.
Lo, S. F., Miller, V. P., Lei, Y., Thorson, J. S., Liu, H.-w., & Schottel, J. L. (1994) *J. Bacteriol. 176*, 460−468.
Lüderitz, O., Staub, A. M., & Westphal, O. (1966) *Bacteriol. Rev. 30*, 192−248.
Marsh, E. N. G. (1995) *Bioessays 17*, 431−441.
Massey, V., & Ghisla, S. (1974) *Ann. NY Acad. Sci. 227*, 446−465.
Matsuzaki, R., Suzuki, S., Yamaguchi, K., Fukui, T., & Tanizawa, K. (1995) *Biochemistry 34*, 4524−4530.
Medda, R., Padiglia, A., Pedersen, J. Z., Rotilio, G., Agrò, A. F., & Floris, G. (1995) *Biochemistry 34*, 16375−16381.
Miles, E. W. (1986) in *Coenzymes & Cofactors: Vitamin B_6 Pyridoxal Phosphate, Chemical, Biochemical, & Medical Aspects. Part B* (Dolphin, D., Poulson, R., & Avramovic, O., Eds.) pp 253−310, John Wiley & Sons, New York.
Miller, V. P., Thorson, J. S., Ploux, O., Lo, S. F., & Liu, H.-w. (1993) *Biochemistry 32*, 11934−11942.
Pedersen, J. Z., El-Sherbini, S., Finazzi-Agrò, A., & Rotilio, G. (1992) *Biochemistry 31*, 8−12.
Ploux, O., Lei, Y., Vatanen, K., & Liu, H.-w. (1995) *Biochemistry 34*, 4159−4168.
Raetz, C. R. H. (1990) *Annu. Rev. Biochem. 59*, 129−170.
Ravi, N., Bollinger, J. M., Jr., Tong, W. H., Huynh, B. H., Edmondson, D. E., & Stubbe, J. (1994) *J. Am. Chem. Soc. 116*, 8007−8014.
Rubenstein, P. A., & Strominger, J. L. (1974a) *J. Biol. Chem. 249*, 3776−3781.
Rubenstein, P. A., & Strominger, J. L. (1974b) *J. Biol. Chem. 249*, 3782−3788.

Schnackerz, K. D., Ehrlich, J. H., Giesemann, W., & Reed, T. A. (1979) *Biochemistry 18*, 3557−3563.
Schnackerz, K. D., Tai, C.-H., Simmons, J. W., Jacobson, T. M., Rao, G. S. J., & Cook, P. F. (1995) *Biochemistry 34*, 12152−12160.
Stevenson, R. C., Dunham, W. R., Sands, R. H., Singer, T. P., & Beinert, H. (1986) *Biochim. Biophys. Acta 869*, 81−88.
Stubbe, J. (1989) *Annu. Rev. Biochem. 58*, 257−285.
Sun, X., Eliasson, R., Pontis, E., Andersson, J., Buist, G., Sjöberg, B.-M., & Reichard, P. (1995) *J. Biol. Chem. 270*, 2443−2446.
Tarr, G. E. (1986) in *Methods of Protein Microcharacterization* (Shively, J. E., Ed.) pp 155−194, Humana Press, Clifton, NJ.
Thorson, J. S., & Liu, H.-w. (1993a) *J. Am. Chem. Soc. 115*, 7539−7540.
Thorson, J. S., & Liu, H.-w. (1993b) *J. Am. Chem. Soc. 115*, 12177−12178.
Thorson, J. S., Lo, S. F., Ploux, O., He, X., & Liu, H.-w. (1994) *J. Bacteriol. 176*, 5483−5493.
Torchinsky, Y. M. (1986) in *Coenzymes & Cofactors: Vitamin B_6 Pyridoxal Phosphate, Chemical, Biochemical, & Medical Aspects. Part B* (Dolphin, D., Poulson, R., & Avramovic, O., Eds.) pp 169−221, John Wiley & Sons, New York.
Wagner, A. F. V., Frey, M., Neugebauer, G. A., Schaefer, W., & Knappe, J. (1992) *Proc. Natl. Acad. Sci. U.S.A. 89*, 996−1000.
Wagner, H.-U., & Gompper, R. (1974) in *The Chemistry of the Quinonoid Compounds* (Patai, S., Ed.) pp 1145−1178, John Wiley & Sons, New York.
Weigel, T. M., Liu, L.-d., & Liu, H.-w. (1992a) *Biochemistry 31*, 2129−2139.
Weigel, T. M., Miller, V. P., & Liu, H.-w. (1992b) *Biochemistry 31*, 2140−2147.
Whittaker, M. M., & Whittaker, J. W. (1990) *J. Biol. Chem. 265*, 9610−9613.
Williams, N. R., & Wander, J. D. (1980) in *The Carbohydrates: Chemistry & Biochemistry, Vol. 1B* (Pigman, W., & Horton, D., Eds.) pp 761−798, Academic Press, New York.
Wu, W., Lieder, K. W., Reed, G. H., & Frey, P. A. (1995) *Biochemistry 34*, 10532−10537.

BI961370W